(article starts on next page)

Modelling of plasma response to three-dimensional external magnetic field perturbations in EAST

Xu Yang[1], Youwen Sun[2], Yueqiang Liu[3, 4, 5, ∗], Shuai Gu[2], Yue Liu[1, ∗], Huihui Wang[2], Lina Zhou[1], Wenfeng Guo[2]

[1] Key Laboratory of Materials Modification by Laser, Ion and Electron Beams, Ministry of Education, School of Physics and Optoelectronic Technology, Dalian University of Technology, Dalian 116024, People's Republic of China

[2] Institute of Plasma Physics, Chinese Academy of Sciences, PO Box 1126, Hefei 230031, People's Republic of China

[3] CCFE, Culham Science Centre, Abingdon, OX14 3DB, UK

[4] Southwestern Institute of Physics, PO Box 432, Chengdu 610041, People's Republic of China

[5] Department of Earth and Space Science, Chalmers University of Technology, SE-412 96 Gothenburg, Sweden

Corresponding authors: yueqiang.liu@ukaea.uk; liuyue@dlut.edu.cn

Abstract

Sustained mitigation and/or suppression of the type-I edge localized modes (ELMs) have been achieved in EAST H-mode plasmas, utilizing the resonant magnetic perturbation (RMP) fields, produced by two rows of magnetic coils located just inside the vacuum vessel. Systematic toroidal modelling of the plasma response to these RMP fields, with various coil configurations (with dominant toroidal mode number n=1, 2, 3, 4) in EAST, is for the first time carried out by using the MARS-F code [Liu Y *et al* 2000 *Phys. Plasmas* **7** 3681], with results reported here. In particular, the plasma response is computed with varying coil phasing (the toroidal phase difference of the coil currents) between the upper and lower rows of coils, from 0 to 360 degrees. Four figures of merit, constructed based on the MARS-F computations, are used to determine the optimal coil phasing. The modelled results, taking into account the

plasma response, agree well with the experimental observations in terms of the coil phasing, for both the mitigated and the suppressed ELM cases in EAST experiments. This study provides a crucial confirmation of the role of the plasma edge peeling response in the ELM control, complementing similar studies carried out for other tokamak devices.

1. Introduction

The edge localized modes (ELMs), driven by the plasma edge pressure gradient and/or current, are rapid repetitive bursts, which occur at the high-confinement (H-mode) regime [1-3]. During recent years, it has been realized that large ELMs, the so-called type-I ELMs [4], can pose significant danger to the material walls in future tokamak devices such as ITER [5]. If not mitigated or suppressed, ELMs can actually damage the wall surfaces, or the divertors which are designed to withhold large thermal load in tokamak devices. Three potential techniques are presently being experimented, and theoretically investigated as well, in order to control the type-I ELMs. One method is to inject fuel pellets into the plasma, which effectively changes the plasma equilibrium and thus affecting the ELM behavior [6]. The second method tries to push the plasma to quickly oscillate along the vertical direction inside the torus. The induced current in the plasma edge helps to modify the plasma edge safety factor, thus changing the so-called peeling-ballooning instability [7, 8], which is responsible for the ELM crash. The last, and so far the most mature and reliable technique, is the application of the resonant magnetic perturbation (RMP) fields. The

ELMs can often be well mitigated [9], or even fully suppressed [10] using the RMP coils.

The RMP technique has been extensively employed in DIII-D [11], JET [12], MAST [13-15], ASDEX-Upgrade [16], and recently in KSTAR [17] as well as EAST [18]. ELM mitigation and/or suppression, with varying success, have been achieved in these devices.

Significant theory and modelling efforts have also been devoted in understanding the physical mechanisms associated with the ELM control with RMPs. The vacuum field approximation [19], adopted in earlier theories, is found to be capable of explaining certain experimental observations. Plasma response based on ideal or resistive MHD models, on the other hand, has been shown to provide good quantitative agreement with experimental data [19-26]. Furthermore, non-linear MHD modelling, using JOREK [27], M3D-C1[28, 29], BOUT++ [30], NIMROD [31], as has been well summarised in Ref. [32] , has provide crucial understanding of the ELM and ELM control physics.

In this work, we carry out computational modelling of the plasma response to three-dimensional external magnetic field perturbations, in EAST tokamak fusion devices, using the MARS-F code [33], which has been well benchmarked [23] and extensively utilized for modelling various RMP experiments in tokamaks worldwide [7, 9, 34-37], including ITER [21]. The key aspects of these toroidal computations are (i) a systematic investigation of the roles of various RMP coil configurations on the plasma response, and (ii) a direct comparison of the modelling results with EAST

experiments, for a series of representative ELM control discharges.

Details of the computational model, used for the RMP response study, are described in Section 2. The EAST plasma equilibria, as well as the RMP coils, are specified in Section 3. Modelling results for representative EAST discharges (52340, 56360, 55272) are reported in Section 4. Section 5 gives the summary and discussion.

2. Computational model

In this work, the plasma response to the RMP fields is described by the single fluid, resistive, full MHD equations including toroidal equilibrium flow, together with the vacuum field and the coil current equations

$$i(\Omega_{RMP} + n\Omega)\xi = \mathbf{v} + (\xi \cdot \nabla\Omega)R\hat{\phi} \tag{1}$$

$$i\rho(\Omega_{RMP} + n\Omega)\mathbf{v} = -\nabla p + \mathbf{j} \times \mathbf{B} + \mathbf{J} \times \mathbf{b} - \rho\left[2\Omega\hat{\mathbf{Z}} \times \mathbf{v} + (\mathbf{v} \cdot \nabla\Omega)R\hat{\phi}\right]$$
$$- \rho\kappa_\parallel\left[k_\parallel\upsilon_{th.i}\right]\left[\mathbf{v} + (\xi \cdot \nabla)\mathbf{V}_0\right]_\parallel \tag{2}$$

$$i(\Omega_{RMP} + n\Omega)\mathbf{b} = \nabla \times (\mathbf{v} \times \mathbf{B}) + (\mathbf{b} \cdot \nabla\Omega)R\hat{\phi} - \nabla \times (\eta\mathbf{j}) \tag{3}$$

$$i(\Omega_{RMP} + n\Omega)p = -\mathbf{v} \cdot \nabla P - \Gamma P\nabla \cdot \mathbf{v} \tag{4}$$

$$\mathbf{j} = \nabla \times \mathbf{b} \tag{5}$$

$$\nabla \times \mathbf{b} = \mathbf{j}_{RMP}, \nabla \cdot \mathbf{j}_{RMP} = 0 \tag{6}$$

$$\nabla \times \mathbf{b} = 0, \nabla \cdot \mathbf{b} = 0 \tag{7}$$

where n is the toroidal harmonic number, R the plasma major radius, $\hat{\phi}$ the unit vector along the geometric torodial angle ϕ of the torus, and $\hat{Z}$ the unit vector in the vertical direction in the poloidal plane. **B**, **J**, P, ρ are the equilibrium plasma magnetic field, current, pressure and density, respectively. **b**, **j**, **v**, p, ξ are perturbed quantities

which represent magnetic field, current, velocity, pressure and plasma displacement, respectively. The parameters η and Γ=5/3 are the plasma resistivity and adiabatic heating coefficient, respectively.

Equations (1)-(5) describe the perturbed MHD equations valid in the plasma region. Equations (5) and (7) describe the vacuum field solution. Finally, equation (6) represents the RMP coil current $\mathbf{j}=\mathbf{j}_{RMP}$, which is assumed to be located in the vacuum region. Note that, in MARS-F, the perturbed magnetic field b and the perturbed current j are defined as global quantities across the plasma-vacuum regions. Equations (1)-(7) are thus self-consistently solved all together, with the boundary condition of vanishing radial field at the computational boundary, which is located far from the plasma (normally a vacuum region of ~6 times larger than the plasma, in terms of the minor radius, is included in MARS-F computations). Proper interface conditions (continuous perturbed radial magnetic field and perturbed kinetic and magnetic pressure balance across the equilibrium plasma boundary) are also imposed at the plasma-vacuum boundary.

The last term in Eq. (2) describes the parallel sound wave damping, where $k_{\parallel}=(n-m/q)/R$ is the parallel wave number and $\upsilon_{th.i}=\sqrt{2T_i/M_i}$ is the thermal ion velocity, with T_i, M_i being the thermal ion temperature and mass. We assume $\kappa_{\parallel}=1.5$ in this work, following arguments from Refs.[6, 26]. In a systematic investigation for the ASDEX Upgrade plasmas [26], it has been shown that a strong parallel sound wave damping ($\kappa_{\parallel}=1.5$) reduces the kink response in the plasma core region, compared to the weak damping model ($\kappa_{\parallel}\ll 1$), without significant

modification to the plasma edge response. Consequently, all the further results (the figures of merit), which are related to the plasma edge and will be reported in this work, are not sensitive to the choice of $\kappa_{\|}$. $\mathbf{V}_0 = R\Omega\hat{\phi}$ is the equilibrium toroidal flow speed, with Ω being the angular frequency of the toroidal rotation. The toroidal flow introduces the Doppler shift effect as evident from Eqs. (1)-(4), combined with the applied RMP coil current frequency Ω_{RMP}. For a static RMP field, which is assumed in this modelling work and which is also the case in EAST experiments (during the flat-top phase of the RMP current), we have $\Omega_{RMP}=0$.

3. Equilibrium and coil configuration

The 2D plasma equilibria used in this study were obtained from the EAST discharges 52340 at $3150\,ms$, 56360 at $2812\,ms$, and 55272 at $4010\,ms$. The EFIT equilibrium code [38] was used for the equilibrium reconstruction. Figure 1 shows one example of the equilibrium flux surfaces for the EAST single-null discharge 52340. Shown are also two rows of the RMP coils, located on the upper ("U") and lower ("L") half-planes, respectively, of the poloidal cross section. Each row consists of 8 window frame coils, equally spaced along the toroidal angle. Each coil covers 37° of the toroidal angle.

With 8 coils distributed along the toroidal angle, the RMP fields with the toroidal mode number up to $n=4$ can be applied. For lower-n configurations (e.g. $n=1, 2$), the toroidal phase difference for the coil currents, between the upper and lower rows, can be discretely varied in experiments. This phase difference, defined as $\Delta\Phi=\Phi_L-\Phi_U$,

shall be referred to as the "coils phasing" [26] in further discussions. For the $n=4$ configuration, on the contrary, only even ($\Delta\Phi=0°$) or odd ($\Delta\Phi=180°$) parity is possible in experiments. In the MARS-F modelling, however, we assume a continuous $exp(in\phi)$ dependence for all perturbed quantities, for a given n number. This allows us to continuously vary the coil phasing for all n's configurations.

In EAST, each coil has 4 turns, with the maximal current of 2.5kA per turn [39]. In MARS-F modelling, we normally assume the same amount of the coil current, although this is not a critical parameter, since all the computed perturbed quantities simply scales linearly with the assumed coil current.
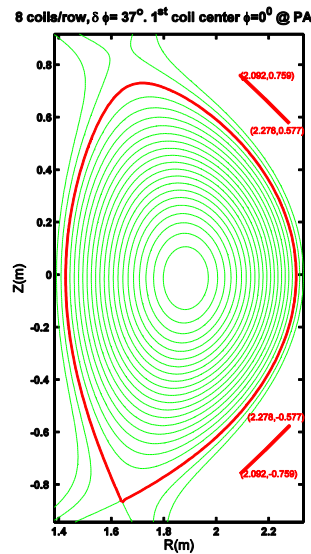

Figure 1. Geometrical location of the upper and lower rows of the ELM control coils in EAST. Each row consists of 8 window frame coils uniformly distributed along the toroidal angle, with each coil's coverage of $\delta\phi=37°$. Shown also are the reconstructed equilibrium flux surfaces for EAST discharge 52340.

Figure 2 shows the radial profiles for the equilibrium safety factor q and the

torodial rotation frequency. Three representative discharges (52340, 56360, 55272) are plotted together. Discharge 52340 is a reference plasma for a series of ELM control experiments (with the best combination of diagnostics for the equilibrium reconstruction). Discharge 56360 utilized the $n=2$ RMP configuration, which assumed two constant coil phasing angles ($\Delta\Phi=90°$ and 270°) during pulse. Discharge 55272 applied the $n=1$ RMP field with varying coil phasing.
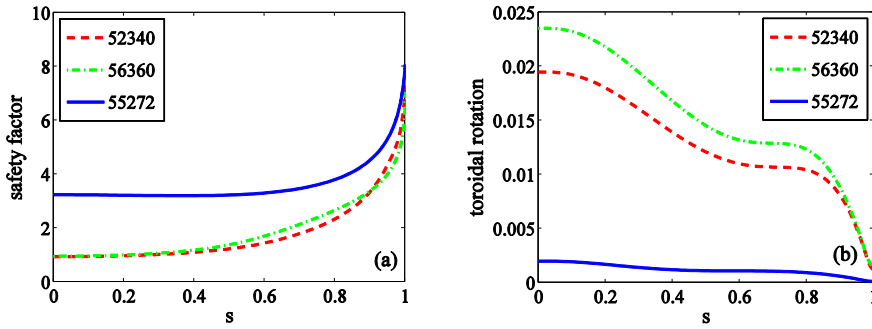

Figure 2. Radial profiles for a set of equilibria studied here and reconstructed from EAST discharges 52340 (dash line), 56360 (dash-dot line), and 55272 (solid line), for (a) the safety factor and (b) the plasma toroidal rotation normalized to the on-axis Alfvén frequency. The radial coordinate s labels the equilibrium poloidal flux surface.

A list of key equilibrium and coil parameters is documented in Table 1 for these three discharges. In the table, R_0 is the plasma major radius. B_0 is the field strength at the magnetic axis. The total plasma current is denoted by I_p. q_0 and q_{95} are the safety factor on the magnetic axis and at the 95% poloidal flux surface, respectively. $\beta_\mathrm{N} \equiv \beta[\%]a[\mathrm{m}]B_0[\mathrm{T}]/I_\mathrm{p}$ is the normalized pressure, with $\beta = (2\mu_0\langle P\rangle)/(B_0^2)$ being the ratio of the volume averaged plasma pressure to the magnetic pressure on axis, and a is the minor radius of the plasma boundary. $\tau_A = (R_0\sqrt{\mu_0\rho_0})/B_0$ is the Alfvén time.

Ω/ω_A is the on-axis ratio of the plasma toroidal rotation frequency to the Alfvén frequency, with $\omega_A=1/\tau_A$. In the next Section, we shall perform the plasma response computations for these three equilibria, assuming the toroidal mode number for the RMP fields as specified in Table 1.

Table 1.Key discharge parameters of EAST shots 52340, 56360, and 55272.

Shot#	Time[ms]	R_0[m]	B_0[T]	I_p[MA]	β_N	q_0	q_{95}	τ_A[μs]	Ω/ω_A	n
52340	3150	1.80	2.30	0.40	1.05	0.950	5.08	0.31	1.95e-2	1,2,3,4
56360	2812	1.75	1.85	0.41	1.15	0.961	4.59	0.37	2.35e-2	2
55272	4010	1.80	2.23	0.42	0.70	3.250	6.07	0.32	2.01e-2	1

4. Modelling results for EAST plasmas

4.1. Definitions of figures of merit for the plasma response

The ELM mitigation/suppression depends on the choice of the coil phasing, as has been observed in EAST RMP experiments (see below). In order to relate the experimental results to the modelled plasma response, we need to define certain criteria, or figures of merit (FoM). Previous toroidal modelling for MAST [21] and ASDEX Upgrade [19, 26] has revealed several relevant quantities, that can be used for this purpose. In the following, we define these figures of merit.

The first two FoM are based on the resonant harmonic of the radial magnetic perturbations in a straight field line coordinate system (with the toroidal angle being the geometrical one and with the poloidal angle chosen such that the Jacobian is $J=q\psi'R^2/F$, where the derivative is with respect to the minor radial coordinate, and F

is the equilibrium poloidal current flux function.). More specifically, we define the amplitude of resonant harmonic of either the vacuum field perturbation , or the total perturbation including the MARS-F computed plasma response, at the last rational surface close to the plasma boundary, for a given toroidal mode number

$$b_{res}^{1} = \left| \left(\frac{\mathbf{b} \cdot \nabla \psi}{\mathbf{B}_{eq} \cdot \nabla \phi} \right)_{mn} \right| \frac{1}{R_0^2}$$

where $\mathbf{b}$ is perturbed magnetic field, ψ the equilibrium poloidal magnetic flux, and $\mathbf{B}_{eq}$ the equilibrium field. The reason that we can choose the last rational surface is our truncation of the exact X-point in the equilibrium plasma boundary, by slightly smoothing the boundary shape near the X-point (a similar approach, often adopted in literatures, is to truncate a small fraction of the poloidal flux near the separatrix). The X-point smoothing procedure results in a finite edge q value.

The next two FoM are associated with the normal displacement of the plasma surface. This is also often referred to as the plasma surface corrugations in literatures. The plasma displacement is caused by the plasma response to the applied RMP field. We shall therefore not discuss the plasma displacement associated only with the vacuum field model. We consider the plasma surface displacement near the X-point, as well as at the outboard mid-plane. Previous comparison between the MARS-F modelling results and the MAST experiments [21] shows that the most relevant quantity, for interpreting the RMP induced density pumpout effect (which normally accompanies the ELM mitigation in MAST), is the ratio of the magnitude between the X-point point displacement and the mid-plane displacement. In other words, for a given RMP coil current, the largest effect on the type I-ELMs is achieved in MAST,

when the X-point displacement is maximized whist the outboard mid-plane displacement is minimized. In AUDEX Upgrade low collisionality ELM control experiments, we found that the best ELM mitigation occurs when the X-point displacement is maximized, and/or when the resonant field harmonic amplitude at the last rational surface close to the plasma surface, including the plasma response, is maximized [19, 26].

4.2. Systematic scan of the coil phasing for reference discharge 52340

We start the investigation by modelling the reference discharge 52340. We scan the coil phasing for $n=1, 2, 3, 4$, while monitoring the two field perturbation based figures of merit as defined in the previous subsection. The results are summarized in Fig. 3. Figure 3(a) shows the magnitude of the pitch-resonant radial magnetic perturbation at the last rational surface close to the plasma surface, for the $n=1$ RMP configuration. Compared are the vacuum field (blue square dashed line) and the total perturbation field including the plasma response (red circle solid line). The maximum value of the vacuum field occurs at $\Delta\Phi\sim315°$，whereas the maximum value of the total response field occurs at $\Delta\Phi\sim15°$. The plasma response introduces a 60° (or -300°) offset for the optimal $\Delta\Phi$ (that maximizes b_{res}^1).

For the $n=2$ coil configuration (Fig. 3(b)), including the plasma response, the maximum of the magnetic perturbation field occurs at $\sim270°$. Considering the vacuum field alone, the maximum occurs at $\sim195°$. The offset in the optimal coil phasing is about 75°. Figure 3(c) shows the corresponding results for the $n=3$ configuration. The

optimal coil phasing is $\Delta\Phi=60°$ in the vacuum approximation, and $\Delta\Phi=135°$ with the plasma response. The offset is again 75°. Interestingly, almost the same offset of 75° is also computed for the $n=4$ coil configuration (Fig. 3(d)), despite the fact the optimal coils phasing (either for the vacuum field or for the total response field) significantly varies for different n's.
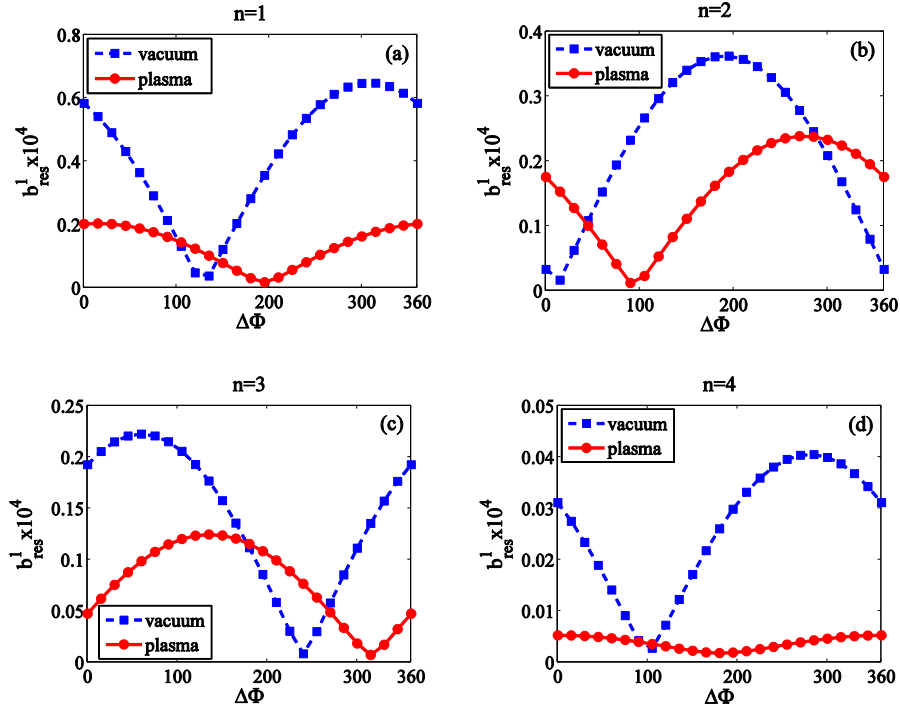

Figure 3. The MARS-F computed amplitude of the perturbed resonant radial field component at the last rational surface close to the plasma boundary, plotted versus the coil phasing (the toroidal phase difference for the RMP coil currents between the upper and the lower rows of coils). Modelling is performed for EAST discharge 52340, assuming various coil configurations yielding dominant field component with the toroidal mode number (a) $n=1$, (b) $n=2$, (c) $n=3$, (d) $n=4$. The vacuum RMP field perturbation (squares) is compared to the total field perturbation including the plasma

response (circles).

4.3. Comparison between modelling and experiments for discharge 56360

ELM control was carried out in EAST discharge 56360, with the experimental observations summarized in Fig. 4. The RMP coils, in the $n=2$ configuration, are applied during 3.1-4.6s of the discharge, splitted into two periods with different coil phasing (270° during 3.1-3.9s and 90° during 3.9-6.4s, Fig. 4(c)). The RMP effects on ELMs (Fig. 4(a)) and the electron density (Fig. 4(b)) are drastically different. In particular, the 270° coil phasing results in clear increase of the ELM frequency (i.e. mitigation effect), causing a large density pumpout, whilst the 90° coil phasing has little effect on the ELMs behavior and on the plasma parameters.
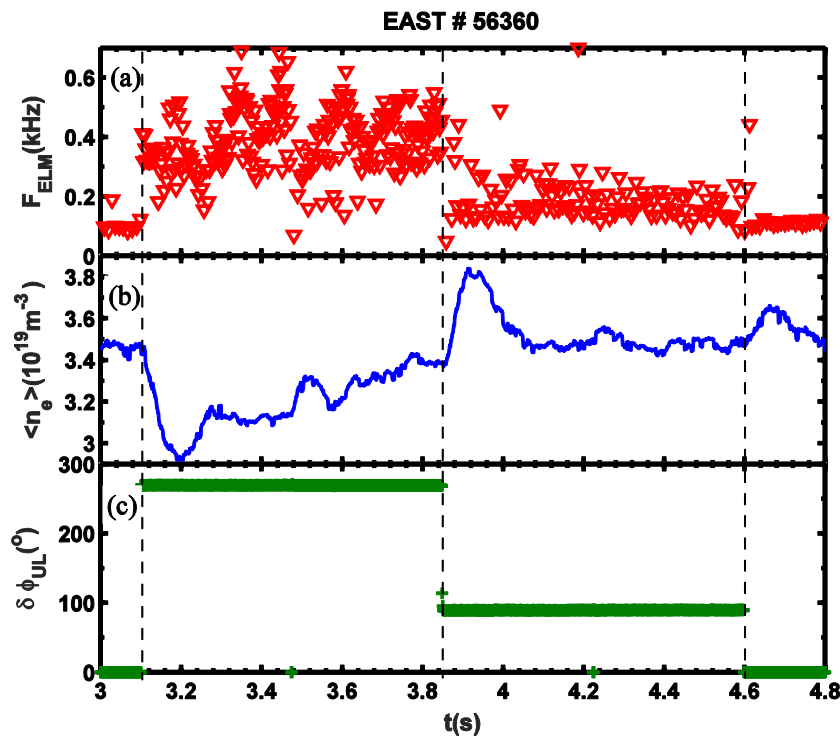

Figure 4. Summary of experimental results for the ELM control discharge 56360, using the $n=2$ RMP coil configuration with two choices of the coil phasing ($\Delta\Phi=90°$

13

and 270°). Shown are the time traces for (a) the estimated ELM frequency, (b) the line-averaged electron density, (c) different coil phasing $\Delta\Phi=270°$ during 3.1-3.9s and $\Delta\Phi=90°$ during 3.9-6.4s.

However, if we compare the poloidal spectrum of the vacuum field between 90° and 270° coil phasing, we find that the 90° gives much larger resonant spectrum than the 270° phasing, as shown by Figs. 5(a) and (c). The vacuum spectrum thus predicts the opposite effect as observed in experiments (Fig. 4). This seemingly counter-intuitive result is resolved by taking into account the plasma response. Indeed, Figs. 5(b) and (d) show that, the total resonant response field, even though being shielded due to the plasma response with both 90° and 270° coil phasing, the 270° phasing gives larger b^1_{res}. This is more clearly seen in Fig. 6, where we scan the coil phasing between 0° and 360°. In fact not only that the 270° coil phasing gives a larger b^1_{res} compared to the 90°, when the plasma response is included (Fig. 6(a)), the plasma surface displacement near the X-point and near the outboard mid-plane is also larger with 270° (Fig. 6(b)). These results, that better ELM mitigation is achieved with the coil phasing that maximizes the resonant field component near the plasma edge, and/or the plasma surface displacement near the X-point, are the same as those obtained for the AUDEX Upgrade plasmas [9, 19, 26], where the $n=2$ RMP fields are applied to mitigate the type-I ELMs.
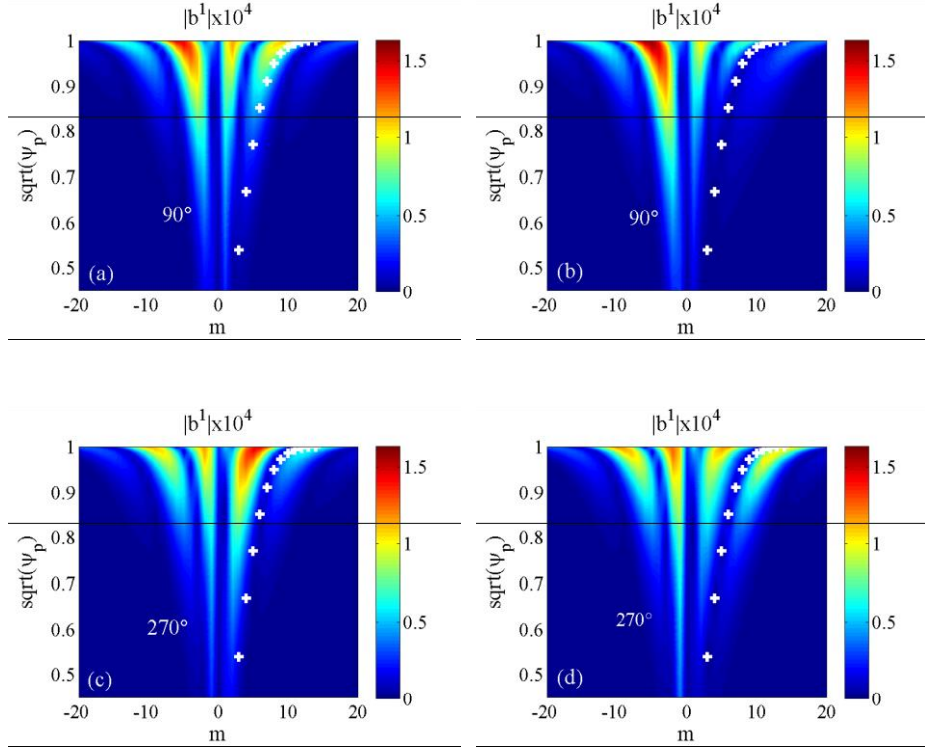
Figure 5. Comparison of the poloidal spectrum of the perturbed radial magnetic field, between the vacuum field (left panel) and the total field including the plasma response (right panel), and assuming the coil phasing of $\Delta\Phi=90°$ (upper panel) and $\Delta\Phi=270°$ (lower panel), respectively. The $n=2$ RMP field is applied to the EAST 56360 plasma. The symbols '+' indicate the location of the $q=m/n$ rational surfaces.
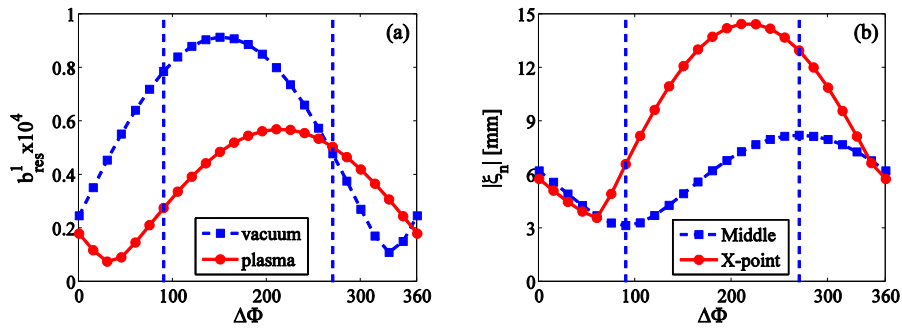

Figure 6. The MARS-F computed figures of merit versus the coil phasing for the EAST discharge 56360, assuming the $n=2$ RMP configuration, for (a) the perturbed resonant radial field amplitude at the last rational surface including the vacuum only

(squares) and including the plasma response (circles), and (b) the normal displacement amplitude of the plasma surface near the X-point (circles) and at the outboard mid-plane (squares). Vertical lines indicate the experimental choices of the coil phasing ($\Delta\Phi=90°$ and 270°).

4.4. Comparison between modelling and experiments for 55272

Complete type-I ELM suppression is one of the most exciting experimental results, that have recently been achieved in EAST, using the $n=1$ RMP field [18]. Even more interestingly, it has been found that the suppression, which is well reproducible during the shots, sensitively depends on the coil phasing, as shown by Fig. 7. The coil phasing, that allows to achieve the suppression, varies within a band of $\Delta\Phi=55°$ ~120° (Fig. 7(b)). During the suppression, substantial density pumpout, up to 25%, is observed. Interestingly, this band of coil phasing excellently aligns with the range that maximizes b_{res}^1 associated with the plasma response (dashed curve in Fig. 7(c)). The vacuum field computed by the MAPS code, on the other hand, does not predict the best coil phasing for the ELM suppression.

At this point, we emphasize that the same plasma response model (single fluid resistive MHD with plasma flow) has been used to study both the mitigated ELM case (56360) and the suppressed case (55272). The same model seems to be successful in predicting the optimal coil phasing for both cases. The optimal coil phasing is rather different between these two cases (~270° for mitigation and ~90° for suppression), largely due to the difference in the n-number, but also partly due to the difference in

the flow amplitude – the suppressed case has a very slow plasma flow as shown in Fig. 2(b). However, this good match between the modelled optimal coil phasing, and that observed in experiments, does not necessarily mean that exactly the same physics applies to the mitigated and the suppressed cases. The actual suppression physics may be more subtle, but the MARS-F model seems to be capable of catching at least the zero-order effect.
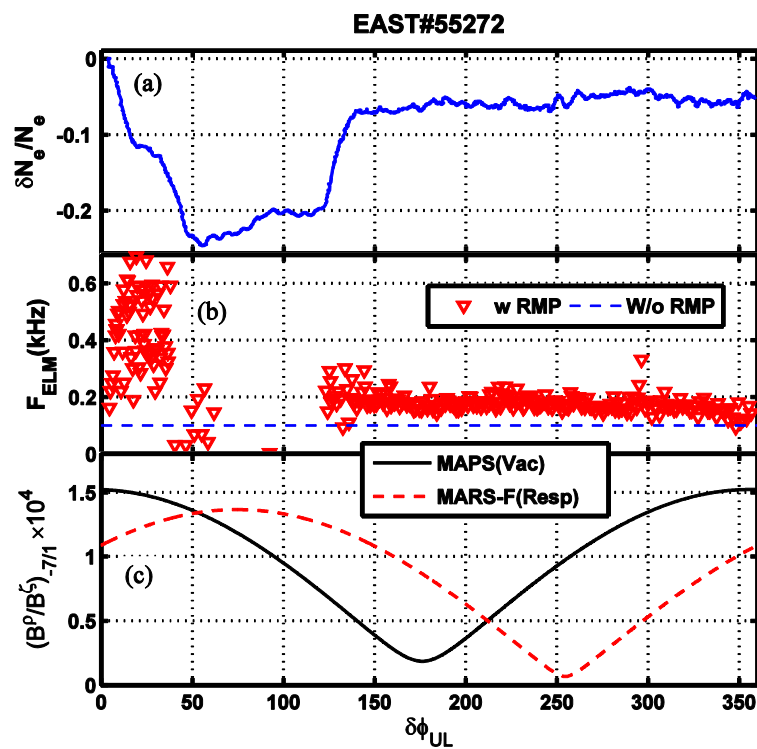

Figure 7. The ELM suppression achieved in EAST discharge 55272, with RMPs in the *n*=1 configuration. Shown are various quantities versus the coil phasing for (a) the electron density pump-out, (b) the frequency of the ELMs, and (c) the computed resonant radial field perturbation at the last resonant surface, comparing the vacuum field (solid line) and the total perturbation including the plasma response (dashed line).

More detailed modelling results are reported in Figs. 8-10. Figure 8(a) compares b_{res}^1 at the last resonant surface between the vacuum and the total response field, with both being computed by MARS-F. The vacuum field matches well the MAPS result shown in Fig. 7(d) (solid line). The best coil phasing, taking into account the plasma response, is $\Delta\Phi=60°$. The same coil phasing also maximizes the X-point displacement, as shown by Fig. 8(b).
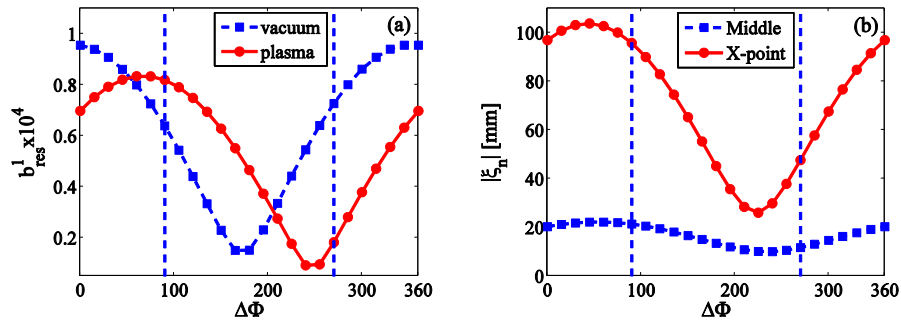

Figure 8. The MARS-F computed figures of merit for EAST shot 55272, assuming the $n=1$ RMP field configuration, versus the coil phasing $\Delta\Phi$ between the upper and lower rows of coils. Compared are (a) the magnitude of the perturbed resonant radial field component at the last rational surface between the vacuum field (squares) and the total field including the plasma response (circles), and (b) the plasma surface displacement between the X-point (circles) and outboard mid-plane (squares). Vertical lines indicate the coil phasing of $\Delta\Phi=90°$ and 270°, respectively.

Figure 9 compares the poloidal spectrum of the vacuum field and the total response field, for two choices of the coil phasing $\Delta\Phi=90°$ and $\Delta\Phi=270°$. Clearly the 90° phasing leads to larger plasma response (in terms of both the total response b_{res}^1 and the X-point displacement) compared to the 270° phasing. Another interesting

observation, shown in Fig. 9(b), is the large amplification of the non-resonant harmonics ($m>0$) at the 90° coil phasing. This is now often referred to as the kink response in literatures [21]. No such kink amplification is obtained with 270° phasing. Note that, compared to the vacuum field, certain degree of the kink amplification is also seen for the non-resonant harmonics with the opposite pitch ($m<0$).
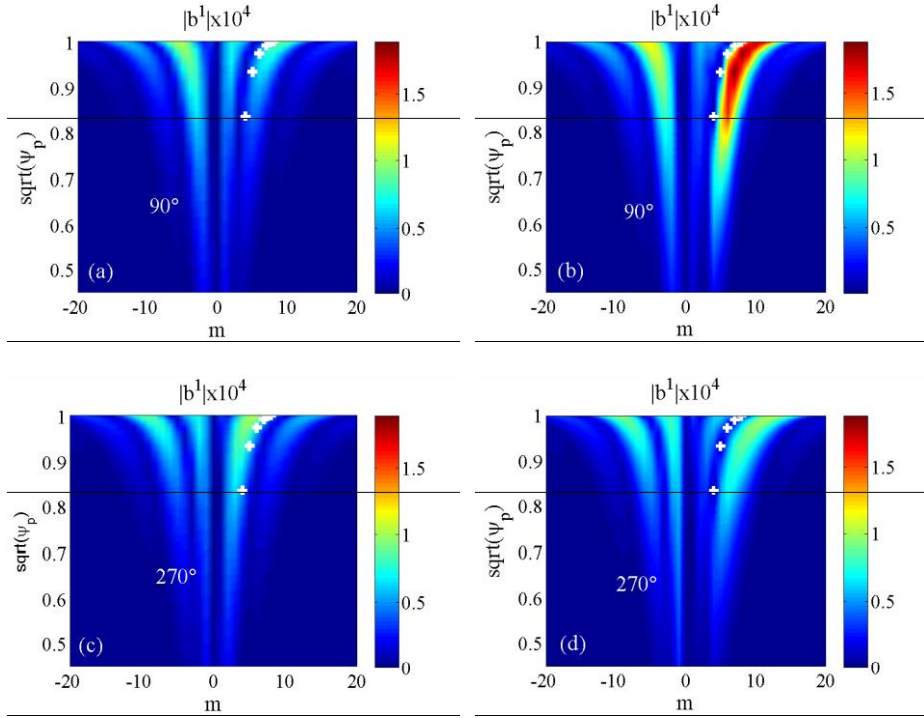

Figure 9. Comparison of the poloidal spectrum of the perturbed radial magnetic field, between the vacuum field (left panel) and the total field including the plasma response (right panel), and assuming the coil phasing of $\Delta\Phi=90°$ (upper panel) and $\Delta\Phi=270°$ (lower panel), respectively. The $n=2$ RMP field is applied to the EAST 55272 plasma. The symbols '+' indicate the location of the $q=m/n$ rational surfaces.

The structure of the whole plasma surface displacement can be mapped onto a plane as shown in Fig. 10. Again it is evident that the largest displacement occurs near

the X-point, corresponding to the poloidal angle of about -100°, with the 90° coil phasing (Fig. 10(a)). Certain displacement also occurs at the top of the torus, with the poloidal angle about +100°. With the 270° coil phasing (Fig. 10(b)), when no ELM suppression was achieved in experiments, much weaker X-point displacement is computed. This correlation is the same as the previous one found with from the ELM mitigation experiments [21]. On the basis of the above discussion, we claim that a better ELM control can be achieved, if the plasma response to the applied RMP field maximizes the X-point displacement. The corresponding optimal coil phasing is documented in Table 2, for all three equilibria studied in this work.
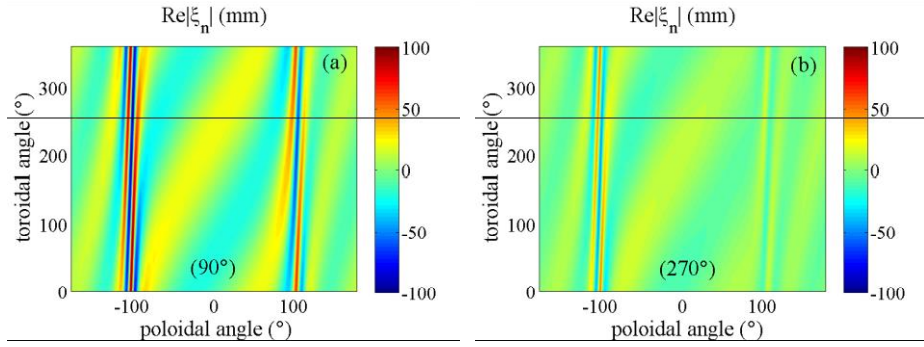

Figure 10. Comparison of the 2D plots of the computed plasma surface displacement, between the coil phasing of (a) $\Delta\Phi=90°$ and (b) $\Delta\Phi=270°$. The $n=1$ RMP field is applied to the EAST 55272 plasma in this case.

Table 2. The MARS-F computed optimal coil phasing $\Delta\Phi$ that maximizes the figures of merit based on the **vacuum** approximation (the resonant radial field component at the last rational surface) and on the **plasma** response model (both the pitch-resonant radial field at the last rational surface close to the plasma surface, and the plasma

surface displacement near the X-point).

Shot#	n	β_N	q_0	q_{95}	vacuum	plasma
52340	1	1.05	0.950	5.08	315°	15°
52340	2	1.05	0.950	5.08	195°	270°
52340	3	1.05	0.950	5.08	60°	135°
52340	4	1.05	0.950	5.08	285°	0°
56360	2	1.15	0.961	4.59	150°	210°
55272	1	0.70	3.250	6.07	345°	60°

5. Summary and discussion

The type-I ELMs are either mitigated or completely suppressed in EAST H-mode，low-collisionality plasmas, using the RMP fields produced by two rows of magnetic coils located just inside the vacuum vessel. Similar to other experiments (MAST, ASDEX Upgrade，and DIII-D), it is found that the mitigation/suppression is sensitive to the choice of the relative coil phasing between the upper and lower rows of the ELM control coils.

This work focuses on toroidal modelling of these ELM control experiments in EAST. Specifically, we use the MARS-F code to perform systematic toroidal computations of the plasma response for representative plasmas chosen from these ELM control experiments. Four figures of merit are constructed from the MARS-F computations, namely the amplitude of the resonant radial field harmonic at the last

rational surface close to the plasma boundary, from either the vacuum RMP field or the total response field, the magnitude of the plasma surface displacement (corrugation) either near the X-point or at the outboard mid-plane. These figures of merit have been extensively considered in the past in order to determine the optimal coil phasing in ELM control experiments in MAST [35] and ASDEX Upgrade [9, 19]. The modelling results, obtained in this work for EAST plasmas, again lead to the conclusion that those plasma response based figures of merit, in particular the pitch-resonant radial field harmonic amplitude at the last rational surface close to the plasma surface and the X-point displacement, predict the optimal coil phasing that agrees with the experimental observations. This provides an important confirmation of the role of the edge peeling response for the ELM mitigation, found in similar studies for other ELM control experiments (MAST [21], ASDEX Upgrade [19, 26, 40] , DIII-D [24, 41]).

The second important finding from the present study is that the field and plasma displacement based criteria, derived from the MARS-F model, seem to work not only for the ELM mitigation, but also for the ELM suppression. This study provides the first such an example. For the EAST H-mode plasmas considered in this work, the optimal coil phasing, according to the plasma response based figures of merit, is about $15°$-$60°$ for the $n=1$ RMP coil configurations, and about $195°$-$270°$ for the $n=2$ coil configuration, aligning well with the experimental results for the ELM suppression ($n=1$) and mitigation ($n=2$). The optimal coil phasing predicted by the vacuum field based criterion, on the other hand, does not agree with experiments. In fact the offset

in the optimal coil phasing, as predicted by the vacuum and by the plasma response field based criteria, is between 60°-75° for all cases considered in this work. This is in excellent agreement with what has been found in ASDEX Upgrade [19]. The optimal coil phasing, found from the modelling results for EAST, can be used to guide further ELM control experiments. This is the third important conclusion from the present study.

Finally, we remark that, even though the MARS-F linear resistive MHD response computations yield agreement, in terms of the coil phasing, with the experimental observations for both ELM mitigation and suppression, the present MARS-F model does not seem to be capable of catching the more subtle physics differences between mitigation and suppression. Work is going-on to further upgrade the model, in order to investigate these differences.

Acknowledgements

References

[1]   Tanga A *et al* 1987 *Nucl. Fusion* **27** 1877

[2]   Zohm H 1996 *Plasma Phys. Control. Fusion* **38** 105

[3]   Connor J W 1998 *plasma Phys. Control. Fusion* **40** 531

[4]   Wagner F *et al* 1982 *Phys. Rev. Lett.* **49** 1408-1412

[5]   Loarte A *et al* 2007 *Nucl. Fusion* **47** S203-S263

[6]   Lang P T *et al* 2004 *Nucl. Fusion* **44** 655

[7]   Liu Y *et al* 2010 *Plasma Phys. Control. Fusion* **52** 045011

[8]   Liu Y *et al* 2010 *Phys. Plasmas* **17** 122502

[9]   Kirk A *et al* 2015 *Nucl. Fusion* **55** 043011

[10]   Wade M R *et al* 2015 *Nucl. Fusion* **55** 023002

[11]   Evans T E *et al* 2004 *Phys. Rev. Lett.* **92** 235003

[12]   Liang Y *et al* 2007 *Phys. Rev. Lett.* **98** 265004

[13]   Nardon E *et al* 2009 *Plasma Phys. Control. Fusion* **51** 124010

[14]   Kirk A *et al* 2010 *Nucl. Fusion* **50** 034008

[15]   Kirk A *et al* 2011 *Nucl. Fusion* **53** 043007

[16]   Suttrop W *et al* 2011 *Phys. Rev. Lett.* **106** 225004

[17]   Jeon Y M *et al* 2012 *Phys. Rev. Lett.* **109** 035004

[18]   Sun Y *et al* 2016 *Phys. Rev. Lett.,* in press

[19]   Ryan D A *et al* 2015 *Plasma Phys. Control. Fusion* **57** 095008

[20]   Lanctot M J *et al* 2011 *phys. Plasmas* **18** 056121

[21]   Liu Y *et al* 2011 *Nucl. Fusion* **51** 083002

[22]   Liu Y Q *et al* 2012 *Plasma Phys. Control. Fusion* **54** 124013

[23]   Turnbull A D *et al* 2013 *Phys. Plasmas* **20** 056114

[24]   King J D *et al* 2015 *Phys. Plasmas* **22** 112502

[25]   Wang Z R *et al* 2015 *Phys. Rev. Lett.* **114** 145005

[26]   Liu Y *et al* 2016 *Nucl. Fusion* **56** 056015

[27]   Czarny O *et al* 2008 *J. Compuy. Phys.* **227** 7423-7445

[28]   Jardin S C *et al* 2007 *J. Compuy. Phys.* **226** 2146

[29]   Ferraro N M *et al* 2010 *Phys. Plasmas* **17** 102508

[30]   Dudson B D *et al* 2009 *Comput. Phys. Commun.* **180** 1467

[31]   Pankin A Y *et al* 2007 *Plasma Phys. Control. Fusion* **49** S63-S75

[32]   Huijsmans G T A *et al* 2015 *Phys. Plasmas* **22** 021805

[33]   Liu Y Q *et al* 2000 *Phys. Plasmas* **7** 3681

[34]   Liu Y *et al* 2009 *Plasma Phys. Control. Fusion* **51** 115005

[35]   Kirk A *et al* 2011 *Plasma Phys. Control. Fusion* **53** 065011

[36]   Liu Y *et al* 2014 *Plasma Phys. Control. Fusion* **56** 104002

[37]   Thornton A J *et al* 2014 *Nucl. Fusion* **54** 064011

[38]   Lao L L *et al* 2005 *Fusion Sci. Technol.* **48** 968

[39]   Sun Y *et al* 2015 *Plasma Phys. Control. Fusion* **57** 045003

[40]   Li L *et al* 2016 *Nucl. Fusion,* in press

[41]   Paz-Soldan C *et al* 2015 *Phys. Rev. Lett.* **114** 105001